Karsili, T. N. V., Wenge, A. M., Marchetti, B., & Ashfold, M. N. R. (2014). Symmetry matters: photodissociation dynamics of symmetrically versus asymmetrically substituted phenols. *Physical Chemistry Chemical Physics*, *16*(2), 588-598. https://doi.org/10.1039/c3cp53450b

Symmetry matters: photodissociation dynamics of symmetrically *versus* asymmetrically substituted phenols

Tolga N.V. Karsili, Andreas M. Wenge[+], Barbara Marchetti and
Michael N.R. Ashfold*

School of Chemistry, University of Bristol, Cantock's Close, Bristol, U.K. BS8 1TS

No. of Figures: 8
No. of Tables: 2

[†] Electronic supplementary information (ESI) available: See DOI:10.1039/c2cp??????

*Corresponding author contact details:

mike.ashfold@bris.ac.uk
Tel: +44 (117) 928 8312
Fax: +44 (117) 925 0612

[+] Present address:
Carl Zeiss SMT GmbH, Rudolf-Eber-Straße 2, 73447 Oberkochen, Germany

ABSTRACT

We report a combined experimental (H (Rydberg) atom photofragment translational spectroscopy) and theoretical (*ab initio* electronic structure and vibronic coupling calculations) study of the effects of symmetry on the photodissociation dynamics of phenols. Ultraviolet photoexcitation to the bound $S_1(^1\pi\pi^*)$ state of many phenols leads to some O–H bond fission by tunneling through the barrier under the conical intersection (CI) between the S_1 and dissociative $S_2(^1\pi\sigma^*)$ potential energy surfaces in the R_{O-H} stretch coordinate. Careful analysis of the total kinetic energy release spectra of the resulting products shows that the radicals formed following $S_1 \leftarrow S_0$ excitation of phenol and symmetrically substituted phenols like 4-fluorophenol all carry an odd number of quanta in vibrational mode ν_{16a}, whereas those deriving from asymmetrically substituted systems like 3-fluorophenol or 4-methoxyphenol do not. This contrasting behavior can be traced back to symmetry. Symmetrically substituted phenols exist in two equivalent rotamers, which interconvert by tunneling through the barrier to OH torsional motion. Their states are thus best considered in the non-rigid G_4 molecular symmetry group, wherein radiationless transfer from the S_1 to S_2 state requires a coupling mode of a_2 symmetry. Of the three a_2 symmetry parent modes, the out-of-plane ring puckering mode ν_{16a} shows much the largest interstate coupling constant in the vicinity of the S_1/S_2 CI. The nuclear motions associated with ν_{16a} are orthogonal to the dissociation coordinate, and are thus retained in the radical products. Introducing asymmetry (even a non-linear substituent in the 4-position) lifts the degeneracy of the rotamers, and lowers the molecular symmetry to C_s. Many more parent motions satisfy the reduced (a'') symmetry requirement to enable S_1/S_2 coupling, the most effective of which is OH torsion. This motion 'disappears' on O–H bond fission; symmetry thus imposes no restriction to forming radical products with vibrational quantum number v=0. The present work yields values for the O–H bond strengths in 3-FPhOH and 4-MeOPhOH, and recommends modest revisions to the previously reported O–H bond strengths in other asymmetrically substituted phenols like 3- and 2-methylphenol and 4-hydroxyindole.

1. INTRODUCTION

The dynamics of photoinduced bond fissions in heteroatom containing aromatic molecules like azoles, phenols, *etc* have been the focus of intensive recent study, both from their perspective of fundamental photochemistry and because many such species constitute the chromophores in larger biochemically relevant species (*e.g.* in the DNA nucleobases).[1-9] The interplay between optically 'bright' states formed via $\pi^*\leftarrow\pi$ excitations ($^1\pi\pi^*$ states), which are bound in all coordinates, and 'dark' $^1\pi\sigma^*$ states which are typically dissociative along the X–H (X = N, O, *etc*) bond extension coordinate ($R_{X–H}$) is crucial to understanding the underlying dynamics.[1, 2, 10-12] In the specific case of phenol (PhOH), the diabatic $1^1\pi\pi^*$ (henceforth S_1) and dissociative $1^1\pi\sigma^*$ (S_2) potential energy surfaces (PESs) display a conical intersection (CI) at planar geometries, at an energy E ~5.4 eV above the ground (S_0) state minimum (*i.e.* ~0.9 eV above the S_1 minimum) and $R_{O–H}$ ~1.2 Å. The S_2 PES shows another CI, with the S_0 PES, at more extended bond lengths ($R_{O–H}$ ~2.1 Å) These features have been described in detail in previous publications;[13-16] analogous PESs for the substituted phenols of current interest will be presented later in this work.

H (Rydberg) atom photofragment translational spectroscopy (HRA-PTS) studies of the UV photodissociation of phenol confirm O–H bond fission following excitation at energies both below and above the CI between the S_1 and S_2 PESs. The total kinetic energy release (TKER) spectrum of the H atom plus ground state phenoxyl (PhO(X)) radical products formed when exciting at the S_1–S_0 origin (*i.e.* to the S_1(v=0) level) shows that the latter are formed in a select set of vibrational levels, with relative probabilities that (in large measure) can be understood on Franck-Condon grounds, given the changes in equilibrium geometry as the S_1 molecules evolve to products. Higher S_1(v) levels are populated upon tuning to shorter wavelengths. Franck-Condon considerations dictate that these mainly involve ring breathing motions (reflecting the softening of the ring upon $\pi^*\leftarrow\pi$ excitation), and the PTS studies show a high propensity for such skeletal motions to map through into the PhO(X) products (*i.e.* to act as 'spectators' to the O–H bond fission process). Tuning to yet shorter wavelengths allows direct access to the $S_2(^1\pi\sigma^*)$ PES and prompt dissociation to H +

PhO(X) products. These products are readily distinguishable from those formed following initial excitation of $S_1(v)$ levels by virtue of their much higher TKER.

As noted earlier, the S_1/S_2 CI in PhOH lies ~0.9 eV above the S_1 origin. Dissociation following excitation to the S_1 state occurs, on a nanosecond timescale, by tunneling through the barrier under this CI.[6,13,14,17,18] The magnitude of this barrier, and thus the tunneling rate, can be 'tuned' by introducing π electron donating/withdrawing substituents at appropriate sites on the ring; cyano- (CN-) substitution at the 4-position, for example, reduces the quantum yield for excited state O–H bond fission to the extent that it becomes immeasurable.[19] The S_1 and S_2 states have different electronic symmetries (A' and A'', respectively, in C_s, B_2 and B_1 in the non-rigid molecular group G_4), necessitating the involvement of an appropriate out-of-plane coupling mode to promote tunneling through the barrier under the S_1/S_2 CI between the two states. Earlier theoretical analyses proposed OH torsion (τ_{OH}) as the out-of-plane mode with the largest associated interstate coupling constant.[14,20] Phenol exists in two symmetrically equivalent planar structures, which can interconvert by tunneling through the torsional barrier.[21-23] Recognition of this tunneling necessitates use of the G_4 symmetry group (isomorphous with C_{2v}), wherein τ_{OH} is of inappropriate symmetry to couple the S_1 and S_2 states, and the lowest frequency parent mode of appropriate (a_2) symmetry is ν_{16a} – consistent with the experimental finding that the PhO(X) products from photodissociation of PhOH(S_1) molecules are formed in levels with ν_{16a} = odd.[24]

Here we report further experiment and computational studies of substituted phenols specifically designed to explore the effects of conserving, and breaking, the formal G_4 symmetry on the product vibrational state distributions arising via O–H bond fission. Previous data for phenol [24, 25] and 4-fluorophenol (henceforth 4-FPhOH) [26] is reprised, new results for 3-fluorophenol (3-FPhOH) and 4-methoxyphenol (4-MeOPhOH) presented, and implications for O–H bond fission from the S_1 states of other asymmetrically substituted phenols like 2- and 3-methylphenol [27] and 4-hydroxyindole [28] considered.

2. METHODOLOGY

2.1 Experimental

The experimental set-up has been described previously.[29, 30] Samples of 4-FPhOH, 3-FPhOH and 4-MeOPhOH (Sigma Aldrich, purity >99%) were packed in an inline filter positioned upstream of a pulsed valve (General Valve, series 9) and maintained at temperatures of ~50, ~30 and ~150°C, respectively, in order to generate sufficient vapor pressures for the photodissociation experiments. Each sample was seeded in Ar carrier gas (stagnation pressure ~1 bar), supersonically expanded and skimmed before being intersected by a pulsed photolysis laser beam. 1+1 resonant enhanced multiphoton ionisation (REMPI) spectra were obtained by positioning a Wiley-McLaren time-of-flight (TOF) mass spectrometer assembly around the interaction region and monitoring the parent ion yield as a function of photolysis laser wavelength, λ_{phot}. H atom photofragment excitation (PHOFEX) spectra were measured by introducing 121.6 nm Lyman-α radiation (generated by tripling 364.7 nm radiation in a phase matched Ar/Kr gas mixture) along with the fundamental precursor radiation from which it is derived, delayed such that these 'probe' pulses arrive in the interaction region ~10 ns after the photolysis laser pulse, and monitoring the H^+ ion yield as a function of λ_{phot}.

For the HRA-PTS studies, a third laser pulse at ~366 nm is introduced so that a fraction of the primary H atom photofragments are promoted to Rydberg states with principle quantum number n ~80 by two photon, two colour (121.6 + 366 nm) double resonant excitation via the 2p state. The TOFs of these Rydberg atoms from the interaction volume (defined by the three laser pulses) to the front face of the detector are then measured. An extraction field (~50 V cm^{-1}) is used to remove unwanted H^+ ions formed in the interaction region. The polarisation vector ($\boldsymbol{\varepsilon}_{phot}$) of the photolysis laser radiation was typically aligned at an angle θ = 0°, 90° and 54.7° (defined with respect to the TOF axis) using a double Fresnel rhomb in order to assess the photofragment recoil anisotropy.

2.2 Theory

Except where stated otherwise, MOLPRO Version 2010.1 [31] was used for the reported *ab initio* calculations. The minimum energy geometry of the ground state of 4-FPhOH, 3-FPhOH and 4-MeOPhOH was optimized in the C_s symmetry group using the complete active space self-consistent field (CASSCF) method with Dunning's augmented correlation consistent basis set of triple ζ quality: aug-cc-pVTZ (AVTZ).[32] Transition dipole moments (TDMs) and vertical excitation energies to the first two excited singlet states of each molecule were calculated using a state averaged complete active space self-consistent field (SA-CASSCF) method under the same AVTZ basis set, but with extra even tempered sets of *s* and *p* diffuse functions on the O atoms in order to describe the Rydberg-valence mixing more effectively. The active space in each case was chosen so as to describe all three molecules in as even handed a manner as possible while minimising computational expense. Test calculations showed that an active space comprising 10 electrons in 10 orbitals (10/10) sufficed for PhOH, 4-FPhOH and 3-FPhOH, but that a (12/11) active space was required for 4-MeOPhOH. The 10 orbitals in the former cases were the three ring centred π bonding orbitals and their π* antibonding counterparts, the p_x orbital on the hydroxy O atom, the oxygen centered 3*s* Rydberg orbital and the σ and σ* orbitals associated with the O–H bond. For 4-MeOPhOH, the methoxy centred O(p_x) lone pair was included also. 'Unrelaxed' potential energy cuts (PECs) along $R_{O\text{-}H}$ were computed for the ground, and first two singlet excited states using complete active space with second order perturbation theory (CASPT2), based on a fully SA-CASSCF reference wavefunction with the remainder of the nuclear framework fixed at the optimised ground state geometry. In all cases, a small imaginary level shift of 0.5 a.u. was applied to encourage convergence and circumvent intruder state effects. The CASPT2 scans were then repeated allowing the nuclear framework for all calculated states to relax at each value of $R_{O–H}$; these we term 'relaxed' PECs.

Equation of motion coupled cluster single and double (EOM-CCSD) calculations were also performed at the CASSCF optimized ground state geometry with the AVTZ basis to determine the TDM vectors and associated oscillator strengths, *f*. Anharmonic wavenumbers for the fundamental vibrations of each ground state molecule and radical were calculated at the DFT/B3LYP/6-311+G(*d,p*) level using Gaussian 03.[33]

A further set of EOM-CCSD calculations (using the cc-pVTZ basis set) were then performed to assess which mode(s) are most likely to promote vibronic coupling at the S_1/S_2 CI. 4- and 3-FPhOH each have 33 vibrational degrees of freedom, 4-MeOPhOH has 45. Of these, 10 transform as a'' in 3-FPhOH (14 in 4-MeOPhOH) and thus have the appropriate symmetry (in C_s) to promote coupling between the S_1 and S_2 states. Like phenol,[13] 4-FPhOH has higher symmetry and is properly considered within the non-rigid molecular group G_4, wherein only 3 of its normal coordinates have the correct (a_2) symmetry to couple the $S_1(B_2)$ and $S_2(B_1)$ states in the vicinity of the CI.

Following Vieuxmaire *et al.*,[14] the geometry of the S_1/S_2 CI was first located by stretching the O–H bond from its equilibrium value to long range. Ground state harmonic frequencies at the CI geometry were then calculated at the MP2/6-311+G(*d*, *p*) level in order to determine the mass-weighted Cartesian normal mode displacements (q_x) by orthogonalising the force constant matrix. Dimensionless displacements (Q_x) were then derived using the relationship:

$$Q_x = \left(\frac{\omega_x}{\hbar}\right)^{\frac{1}{2}} q_x \qquad (1)$$

where ω_x is the ground state harmonic wavenumber of mode x calculated at the MP2/6-311+G(*d*, *p*) level of theory.

A set of single point energy calculations was then undertaken at small displacements from planarity in order to construct a set of PECs along the various vibrational displacements Q_x of appropriate $a''(a_2)$ symmetry. These PECs were then fitted to the linear vibronic coupling model introduced by Domcke, Cederbaum and co-workers.[14, 34, 35] In brief, a diabatic potential matrix W for two interacting excited state PESs as a function of a given Q_x (a'') is constructed thus:

$$W(Q_x) = \begin{pmatrix} W_{11} & W_{12} \\ W_{21} & W_{22} \end{pmatrix} = \begin{pmatrix} E_1 + \frac{1}{2}\left(\omega_x^{(0)} + \gamma_x^{(1)}\right)Q_x^2 & \lambda_x Q_x \\ \lambda_x Q_x & E_2 + \frac{1}{2}\left(\omega_x^{(0)} + \gamma_x^{(1)}\right)Q_x^2 \end{pmatrix}, \qquad (2)$$

where $E_1(E_2)$ is the *ab initio* energy of the $S_1(S_2)$ state. The matrix elements of W contain a quadratic coupling term $\gamma_x^{(1)}$ (which accounts for changes in ω_x in the excited state) and the interstate coupling constant, $\lambda_x^{(1)}$, which is the parameter to be

determined by least-squares fitting the eigenvalues of the 2x2 matrix in eq. (2). The coupling strength of a particular mode *x* is then reported by weighting λ_x against the corresponding ω_x value.

3. RESULTS AND DISCUSSION

3.1 *Ab initio* electronic structure calculations.

Figure 1 shows unrelaxed PECs along $R_{O–H}$ for the S_0, S_1 and S_2 states of (a) 4-FPhOH, (b) 3-FPhOH and (c) 4-MeOPhOH calculated for planar geometries at the CASPT2 level. All are very reminiscent of those reported previously for bare phenol.[19] Noteworthy features are the S_1/S_2 and S_2/S_0 CIs, the relative lowering of the S_1 and (particularly) the S_2 PECs in the case of 4-MeOPhOH – the latter reflecting the additional stabilization of the radical formed on O–H bond fission by substituting a good electron donating group like MeO in the 4-position [19] – and, in all cases, the barrier to tunneling under the S_1/S_2 CI from the S_1(v=0) level.

As noted above, 3-FPhOH and 4-MeOPhOH exist as *syn* and *anti* rotamers (reflecting the relative orientation of the O–H bond to the F atom and the O–Me bond, respectively) but, in both cases, the energy separation ($\Delta E_{syn\text{-}anti}$) of the two rotamers in the S_0 state is calculated to be <10 cm^{-1} (at the DFT/B3LYP/6-311+G(*d*,*p*) level of theory) and thus imperceptible on the scale of these plots.

Unrelaxed and relaxed $S_1 \leftarrow S_0$ and $S_2 \leftarrow S_0$ excitation energies returned by the CASPT2 calculations are shown in Table I, along with the available experimental data. The calculated (EOM-CCSD) oscillator strengths accord with previous conclusions regarding the optically 'bright' S_1 and 'dark' S_2 states of phenols. The relaxed calculations also return O–H bond strengths that (after appropriate correction for zero-point energies) are in very good agreement with the bond dissociation energies (D_0) derived by HRA-PTS studies.

3.2 REMPI and H atom PHOFEX spectra.

Parent ion REMPI and H atom PHOFEX spectra for 4-FPhOH have been reported previously, enabling identification of the S_1–S_0 origin (λ = 284.768 nm) and many peaks attributable to population of Franck-Condon active $S_1(v>0)$ levels at wavelengths in the range $284.768 \geq \lambda \geq 274.5$ nm.[26] 1+1 REMPI spectra for jet-cooled samples of (a) 3-FPhOH and (b) 4-MeOPhOH obtained by monitoring the respective parent ion signals are shown in fig. 2. Guided by previous analyses,[26,27] the features in each spectrum can be assigned to excitations via vibrational levels of the S_1 states of both rotamers. The S_1–S_0 origins for *syn*- and *anti*-3-FPhOH are identified at λ = 273.045 and 271.500 nm, respectively. Given the predicted minimal energy separation between these rotamers in the S_0 state (consistent with the very similar origin band intensities in fig. 2(a)), the ~208 cm^{-1} difference in the measured origins is largely attributable to the greater (relative) stability of the *syn*-rotamer in the S_1 state. Broadly similar considerations apply in the case of 4-MeOPhOH, for which the S_1–S_0 origins are identified at λ = 297.066 nm (*syn*) and 297.932 nm (*anti*), with the ~98 cm^{-1} splitting in this case reflecting the greater stabilisation of the *anti*-rotamer in the S_1 state. H atom PHOFEX spectra of 3-FPhOH and 4-MeOPhOH are included in the electronic supplementary information (see ESI† online). Both mirror the respective parent REMPI spectra, showing peaks attributable to both rotamers, but the signal to noise ratio in the former is consistently less good.

3.3 TKER spectra recorded following photodissociation at energies below and above the S_1/S_2 conical intersection.

For each of 4-FPhOH, 3-FPhOH and 4-MeOPhOH, H atom TOF spectra were measured on several of the more prominent S_1–S_0 resonances in the respective 1+1 REMPI spectra and at a number of short wavelengths (corresponding to excitation energies above the S_1/S_2 CI). As usual,[30] these were all converted to TKER spectra using eq. (3)

$$\mathrm{TKER} = \frac{1}{2} m_H \left(1 + \frac{m_H}{m_R}\right)\left(\frac{d}{t}\right)^2, \qquad (3)$$

where m_H and m_R are the masses of the H atom (1.00794 u) and the partner radical (*i.e.* 4-FPhO and 3-FPhO (m_R = 111.09 u) or 4-MeOPhO (m_R = 123.13 u)), d is the distance between the laser interaction region and the front of the detector and t is the measured H atom TOF. A t^{-3} Jacobian was used when re-binning the measured intensities from TOF to TKER space. As usual, we choose to report the latter in cm^{-1} units.

Figure 3 compares TKER spectra obtained following photolysis of PhOH, 4-FPhOH, 3-FPhOH and 4-MeOPhOH at the respective S_1–S_0 origins (of both rotamers in the latter two cases). Each shows a set of peaks in the TKER ~5000-6000 cm^{-1} range, riding on an unstructured background signal. The detail of the latter varies from molecule to molecule and is sensitive to the incident pulse energy but, as previously, can be attributed to H atoms arising from a combination of unintended multiphoton excitations (which, at these wavelengths, are necessarily responsible for the weak tail evident at high TKER) and 'statistical' decay processes occurring on the S_0 PES. The structured component, attributable to one photon induced excited state O–H bond fission,[19, 26, 27, 36] is similar in all cases, with a dominant peak at high TKER (labeled $TKER_{max}$ in fig. 3) and a short sequence of peaks extending to lower TKER; energy conservation dictates that the latter indicate formation of more vibrationally excited radical fragments. Assignment of these features and discussion of the way the spectra evolve when exciting on other S_1–S_0 resonances is reserved for section 3.5. None of these spectra show any sensitivity to the relative orientation of $\boldsymbol{\varepsilon}_{phot}$ to the TOF axis, implying an isotropic distribution of product recoil velocities and a recoil anisotropy parameter, $\beta = 0$.

As with the phenols studied previously,[24-27] another structured feature appears at higher TKER upon tuning to much shorter wavelengths. Figure 4 shows illustrative TKER spectra from photolysis of (a) PhOH, (b) 4-FPhOH, (c) 3-FPhOH and (d) 4-MeOPhOH. Each shows a progression of peaks, the fastest of which we label $TKER_{max}$. The extent of these progressions again indicates that the radical fragments from O–H bond fission are formed in a (limited) range of vibrational levels, and with little rotational excitation. The parent absorption spectra are continuous at these shorter wavelengths, so the TKER spectra shown in figs. 3(c) and 3(d) are necessarily

a superposition of contributions from both rotamers. That these spectra are not noticeably less well resolved than those from 4-FPhOH, for example, further serves to illustrate that the energy splitting between the different rotamers in the S_0 state is small. Again, interpretation of the structure evident in these spectra and its evolution with excitation wavelength is reserved until section 3.5. In contrast to the data taken at long wavelength, the relative showing of the structured signal in these spectra taken at short wavelengths shows a clear (but molecule dependent) sensitivity to the orientation of $\boldsymbol{\varepsilon}_{phot}$ to the TOF axis. As with PhOH,[24] the structured components in the spectra from 4-FPhOH and 4-MeOPhOH are relatively more intense when $\theta = 90°$ ($\beta \sim -0.5$ and ~ -0.2, respectively), whereas the signal from 3-FPhOH is maximal when $\theta = 0°$ ($\beta \sim +0.3$).

3.4 O–H bond dissociation energies, and the dissociation mechanism at long and short excitation wavelengths.

Figure 5(a) shows a plot of $TKER_{max}$, the TKER of the fastest peak in spectra of the H + PhO products formed by photolysis of PhOH at many different excitation wavelengths, versus the photon energy, E_{phot}. All points in such a plot should lie on a straight line with unit gradient if the $TKER_{max}$ feature is associated with a common set of products (*e.g.* H + PhO(X), v=0 products). As noted previously,[24] all of the points measured at long wavelength (*i.e.* at excitation energies below the S_1/S_2 CI) satisfy this expectation, as do the set of points determined when exciting at energies above the S_1/S_2 CI, but the best-fit lines through the two data sets are offset vertically by ~100 cm^{-1}. (The standard deviations on the intercepts obtained by fitting the long and short wavelength data are, respectively, 9.4 cm^{-1} and 8.2 cm^{-1}, *cf.* $1\sigma = 85$ cm^{-1} if all data points are fit to a single line of unit gradient). Such a finding could be explained by assuming that the $TKER_{max}$ peak in all spectra recorded at short wavelengths is associated with formation of radical products with $v > 0$, but there is no mode of PhO with such a low wavenumber.

Thus the offset has been explained [24] by suggesting that the $TKER_{max}$ peaks in spectra recorded at excitation energies below the S_1/S_2 CI are all associated with PhO(X) products carrying one quantum of ν_{16a} (a_2) whilst those formed at short excitation wavelengths all carry a quantum of ν_{16b} (b_1) – two modes whose wavenumbers

differ by 104 cm^{-1}. As described in the Introduction, the formation of PhO(X) products with $v_{16} = 1$ following long wavelength photolysis is now seen as a signature of the vibronic coupling that promotes tunneling through the barrier under the S_1/S_2 CI.[14] The formation of PhO(X) products with $v_{16b} = 1$ when exciting at energies above the S_1/S_2 CI has been rationalized by assuming that excitation to the 'dark' S_2 state gains transition probability by vibronic mixing with a higher lying state of A_1 electronic symmetry. These analyses imply a bond dissociation energy D_0(PhO–H) = 30015±40 cm^{-1}.[24] Prior HRA-PTS studies of C_6D_5OH [25] and 4-substituted phenols like 4-MePhOH [27] and 4-FPhOH [26] found similar offsets between the lines of best-fit in $TKER_{max}$ *vs* E_{phot} plots of data taken at long and short excitation wavelengths, which were rationalized in the same way. The 4-FPhOH studies return an offset of ~120 cm^{-1} (which, again, matches the wavenumber difference between radical modes v_{16a} and v_{16b} (as shown in the ESI†)) and a dissociation energy D_0(4-FPhO–H) = 29370±50 cm^{-1}.[26]

Figure 5(b) shows the corresponding $TKER_{max}$ *vs* E_{phot} plot for 3-FPhOH; the analogous plot for 4-MeOPhOH has been reported previously [19, 37] and is reprised in the ESI.† The long wavelength data in fig. 5(b) is obtained following excitation of specific resonances attributed to the *syn*- and *anti*-rotamers, while the data taken at short wavelengths necessarily involves contributions from both rotamers. All of the data are fit well by a single line of unit gradient. (The 1σ uncertainty on the intercept from a global fit to all data points is 10 cm^{-1}, and the correlation coefficient R^2 = 0.9999). This reaffirms two points. First, that the energy splitting between the S_0 states of the two conformers is small. Second, since the two rotamers are non-equivalent, the relevant molecular point group is now C_s and (in principle) any nuclear motion of *a″* symmetry can promote coupling between the S_1 and S_2 PESs. As shown below, OH torsion provides the largest interstate coupling in this case (and in the case of 4-MeOPhOH). OH torsion is a 'disappearing' mode upon O–H bond fission. The associated angular momentum maps into framework rotation and product orbital motion, and there is no reason why the products appearing at highest TKER should not be H + PhO(X),v=0 radicals. Attributing the $TKER_{max}$ peaks in this way, and invoking the energy conserving relation

$$D_0(\text{ZPhO–H}) = E_{phot} - TKER_{max} \quad (4)$$

yields D_0(3-FPhO–H) = 30540±50 cm^{-1} and D_0(4-MeOPhO–H) = 28620±50 cm^{-1}. Armed with these values, we can now place all of the TKER spectra on an alternative E_{int} energy scale, where

$$E_{int}(\text{ZPhO}) = E_{phot} - D_0(\text{ZPhO–H}) - \text{TKER} \quad (5)$$

is the internal energy of the radical formed upon dissociation. The vibrational energy disposal in the radical products and its dependence on excitation wavelength is discussed in section 3.5.

Table 2 lists the calculated interstate coupling constants (λ_x) at the S_1/S_2 CI in order of decreasing coupling strength (λ_x/ω_x) which provide further support for the above interpretations. The present calculations suggest that each molecule retains a planar minimum energy geometry out to the S_1/S_2 CI ($R_{O–H}$ ~1.21 Å). Figure 6 shows calculated 1-D PECs for the three a_2 symmetry coupling modes in 4-FPhOH (ν_{26}, ν_{25} and ν_{24}, (ν_{16a}, ν_{17a} and ν_{10a} in Wilson notation [38])) and for the three strongest a'' coupling modes of 3-FPhOH. Full sets of calculated PECs for all a'' coupling modes in both 3-FPhOH and 4-MeOPhOH, and depictions of the dominant coupling motion in these two molecules and in PhOH, 4-FPhOH are shown in the ESI.[†] Visual inspection of these PECs suffices to reveal the relative importance of the linear and quadratic contributions to the Q_x dependent splitting. ν_{16a} shows the largest λ_x/ω_x value in 4-FPhOH (consistent with previous predictions and experimental observations in PhOH [13,22]), while O–H torsion is predicted to be the most efficient coupling mode (largest λ_x/ω_x) in both of the asymmetrically substituted phenols.

3.5 Vibrational energy distributions in the radical products formed following O–H bond fission.

Figures 3 and 4 illustrated the qualitatively similar TKER spectra exhibited by all of these phenols following photolysis at ‘long’ and ‘short’ wavelengths. Figures 7 and 8 show a selection of E_{int} spectra obtained following excitation of 3-FPhOH at energies below and above the S_1/S_2 CI, respectively, which allow a more detailed consideration of the vibrational energy disposal in the radical products. Analogous

spectra from photolysis of 4-MeOPhOH are included in the ESI,[†] while data for 4-FPhOH [26] and PhOH [24] have been reported previously.

The spectrum obtained when exciting the S_1–S_0 origin band of the *syn*-rotamer (fig. 7(a)) shows a peak at E_{int} = 0 (assigned to 3-FPhO(X), v=0 products) and weaker features at E_{int} ~340 cm^{-1}, ~500 cm^{-1} and ~850 cm^{-1}. Comparison with the computed (anharmonic) wavenumbers of the various radical modes (ESI[†], Table S1 in the ESI[†], sequenced in Herzberg notation [39]) suggests assignment of these features to population of, respectively, ν_{21} = 1, ν_{19} = 1 and ν_{28} = 2. ν_{21} and ν_{19} both involve significant in-plane C–O wagging motion; the former is reminiscent of PhO radical mode ν_{18b} (Wilson notation [38]) which is active in the corresponding E_{int} spectrum obtained when exciting at the S_1–S_0 origin in PhOH.[24] ν_{28} in 3-FPhO (an out-of-plane (*a″*) ring puckering motion) is reminiscent of ν_{16a} in PhO, (the wavenumber of which is similar in the X state radical and in the S_0 and S_2 states of PhOH, but substantially smaller in the $S_1(^1\pi\pi^*)$ state). The observed short progression in (double quanta) of ν_{28} in fig. 7(a) can be understood by applying a combination of Franck-Condon and symmetry arguments to the $S_1 \rightsquigarrow S_2$ radiationless transfer and subsequent O–H bond fission. The E_{int} spectrum obtained when exciting at the S_1–S_0 origin band of the *anti*-rotamer shows the same product features, with similar relative intensities. The E_{int} spectrum obtained at λ = 270.669 nm (fig. 7(b)) shows a more extensive progression in radical mode ν_{21}, while the largest peak in fig. 7(c) matches with that expected for population of ν_{25} = 1. The latter is the analogue of mode ν_{9b} in PhO, and both of the latter vibrational distributions are most readily explained by assuming that photoexcitation populates the corresponding mode in *syn*-3-FPhOH(S_1), which maps through into the radical as the O–H bond breaks.

E_{int} spectra taken at energies well above the S_1/S_2 CI (fig. 8) show a sequence of peaks, the centre of gravity of which shifts to higher E_{int} with decreasing λ_{phot}. Guided by the earlier studies,[16, 24, 25] we assign this structure in terms of overlapping progressions with intervals of ~500 cm^{-1} and ~1450 cm^{-1}. These are most plausibly assigned to radical modes ν_{19} and ν_7 (close analogues of modes ν_{9b} and ν_{7a} in PhO and 4-FPhO). As before,[26] population of the former can be rationalised in terms of the impulse arising during O–H bond fission, while population of the in-plane ring-

breathing mode ν_7 likely reflects the relative increase in quinoidal character during the evolution from S_0 molecule, through the excited $^1\pi\sigma^*$ state, to radical products.

The E_{int} spectra of the 4-MeOPhO radicals formed in the photolysis of 4-MeOPhOH (shown in the ESI[†]) are broadly similar. Spectra obtained when exciting on the S_1–S_0 origin of the *syn*- and *anti*-rotamers both show a v = 0 peak and intervals consistent with population of radical modes $\nu_{26}(\nu_{18b})$ = 1 and $\nu_{38}(\nu_{16a})$ = 2 – *i.e.* vibrational energy disposals analogous to that seen in the photolysis of 3-FPhOH and, apart from the offset quantum of ν_{16a}, of PhOH itself. As with the other phenols, additional peaks appear when exciting on higher energy resonances (*e.g.* a peak at E_{int} ~520 cm^{-1} attributable to radical mode $\nu_{25}(\nu_{9b})$ = 1 when exciting at λ_{phot} = 294.532 nm). This is classic 'spectator' mode behavior, as can be seen by referring back to the parent REMPI excitation spectrum (fig. 2(b)). E_{int} spectra of the 4-MeOPhO radicals obtained at short wavelengths are also similar to those from photolysis of other phenols (though marginally less clearly resolved), exhibiting structure consistent with selective population of radical modes $\nu_{25}(\nu_{9b})$ and $\nu_{10}(\nu_{7a})$.

3.6 Implications for previous studies of other asymmetrically substituted phenols.

The earlier paper reporting HRA-PTS studies of 2-, 3- and 4-MePhOH [27] contains the sentences 'In contrast to 4-MePhOH, 4-FPhOH and phenol, the peak at highest TKER in spectra [of 3-MePhOH] recorded in both long and short wavelength regimes is given a common assignment. Thus, there is no *a priori* reason why this peak should not be assigned to formation of v = 0 products.' Nonetheless, analogy with the other symmetric phenols persuaded the authors to assume that all products carried a quantum of out-of-plane mode ν_{36}. In light of the present work, it is now clear that the alternative interpretation wherein the observed $TKER_{max}$ peak in each spectrum is attributed to formation of H + 3-MePhO(X), v=0 products would have been correct. The only consequences of such a reassignment are that all of the peak assignments in figs. 8 and 10 of ref. 27 need to be reduced by one quantum of radical mode ν_{36} and the best estimate of the O–H bond strength increased to D_0(3-MePhO–H) = 30265±50 cm^{-1}. Similar arguments almost certainly apply to the case of 2-MePhOH, though the

TKER spectra obtained at short wavelength showed little structure; the appropriately revised value of D_0(*anti*-2-MePhO–H) = 29680±50 cm^{-1}.

The final example to consider here is 4-hydroxyindole, which shows several well resolved TKER spectra attributable to O–H bond fission following excitation near its $^1L_b(^1A')\leftarrow S_0$ origin, but no discernible structure when exciting at energies above the lowest CI with the $^1\pi\sigma^*$ state.[28] Again, analogy with PhOH encouraged assignment of the TKER$_{max}$ peaks in these spectra to formation of radical products carrying one quantum of the 'ν_{16a}-like' out-of-plane motion (ν_{40} in this case). Re-assigning these features to formation of v = 0 radicals would increase the O–H bond strength in 4-hydroxyindole by ~254 cm^{-1}, to 28240±50 cm^{-1}.

4. CONCLUSIONS

The UV photophysics and photochemistry of phenols has attracted much recent interest, not least because of their role as chromophores in a range of biomolecules.[1,5,7,8,18] At a more detailed level, the recent literature contains several papers that address details of the mechanism by which photoexcited $S_1(1^1\pi\pi^*)$ molecules undergo O–H bond fission by tunneling through the barrier under the CI with the dissociative $S_2(1^1\pi\sigma^*)$ PES.[2,13,14,17,19] One key element of these discussions is the finding that the radicals formed following photoexcitation to the S_1 state of PhOH (and other symmetrically substituted phenols) all carry an odd number of quanta of an out-of-plane skeletal vibration (ν_{16a} in the PhO(X) radicals from PhOH). Our most recent analysis [13] rationalised this finding by recognizing that such phenols exist as two equivalent rotamers, which can interconvert by tunneling through the barrier to OH torsion. Such phenols should thus be considered in the non-rigid molecular symmetry group G_4, wherein radiationless transfer from the $S_1(^1B_2)$ to $S_2(^1B_1)$ states requires a coupling mode of a_2 symmetry; amongst the limited set of such modes in PhOH, ν_{16a} provides the largest interstate coupling. Thus this out-of-plane ring puckering motion promotes tunneling to the S_2 PES and, being orthogonal to the dissociation coordinate, carries through into the eventual radical products.

The present joint experimental/theoretical study revisits the photofragmentation dynamics of one symmetrically substituted phenol (4-FPhOH) and extends such studies to two prototypical asymmetrically substituted phenols (3-FPhOH and 4-MeOPhOH). Careful analysis of TKER spectra obtained following $S_1 \leftarrow S_0$ excitation of these asymmetric phenols shows that the resulting radicals do not carry the odd quantum of 'ν_{16a}-like' vibration. 3-FPhOH and 4-MeOPhOH both exist as two, non-equivalent, rotamers and transform as C_s; their S_1 and S_2 states transform as, respectively, A' and A'' and coupling between these states could (in principle) be promoted by any mode of a'' symmetry. OH torsion is shown to provide the strongest interstate coupling in this lower symmetry point group and, since this motion 'disappears' on O–H bond fission, there is no impediment to forming radical products in their ground (v = 0) level. Thus we arrive at a self-consistent description of the way symmetry influences the vibrational energy disposal in the radical products formed by tunneling (in the $R_{O–H}$ stretch coordinate) from the S_1 states of symmetric and asymmetric phenols. The present analysis yields values for D_0(3-FPhO–H) and D_0(4-MeOPhO–H), and implies a need for modest increases in the previously reported O–H bond strengths in other asymmetrically substituted phenols like 3- and 2-methylphenol and 4-hydroxyindole.

Acknowledgments

The authors are very grateful to EPSRC (programme grant EP/G00224X) and the Marie Curie Initial Training Network ICONIC (contract agreement no. 238671) for financial support, and to R.N. Dixon, J.N. Harvey, K.N. Rosser and J.A. Smith for their many and varied contributions to the work described in this paper.

Table 1: Calculated S_1–S_0 and S_2–S_0 transition energies and oscillator strengths and (zero-point corrected) O–H bond strengths for 4-FPhOH, 3-FPhOH and 4-MeOPhOH, listed along with the experimentally determined $T_{00}(S_1–S_0)$ values and dissociation energies.

	CASPT2 calculations		EOM-CCSD calculations		Experiment *
	Unrelaxed / eV	Relaxed / eV	/ eV	Oscillator Strength (*f*)	/ eV
4-FPhOH					
T_e (S_1–S_0)	4.39	4.22	4.82	0.04310	4.35 [26]
T_e (S_2 –S_0)	5.45	5.29	5.60	0.00005	-
D_0 (4-FPhO–H)	4.03	3.69	-	-	3.64 [26]
***syn*-3-FPhOH**					
T_e (S_1–S_0)	4.59	4.41	5.02	0.02216	4.54*
T_e (S_2 –S_0)	5.71	5.64	5.76	0.00001	-
D_0 (3-FPhO–H)	4.08	3.83	-	-	3.79*
***syn*-4-MeOPhOH**					
T_e (S_1–S_0)	4.23	4.21	4.65	0.05116	4.17 [19]
T_e (S_2 –S_0)	5.13	4.79	5.12	0.00061	-
D_0 (4-MeOPhO–H)	3.88	3.57	-	-	3.55*

* This work

Table 2

Interstate coupling constants (λ_x) calculated for each out-of-plane vibrational motion of appropriate symmetry to promote coupling at the S_1/S_2 CI in 4-FPhOH, 3-FPhOH and 4-MeOPhOH, listed in order of the dimensionless coupling strength, λ_x/ω_x. Modes are labeled in Herzberg notation, along with the corresponding Wilson label wherever appropriate.

Mode	λ_x / cm^{-1}	ω_x / cm^{-1}	λ_x/ω_x
4-FPhOH			
ν_{26} (ν_{16a})	72	399	0.18
ν_{25} (ν_{10a})	78	794	0.10
ν_{24} (ν_{17a})	28	886	0.03
3-FPhOH			
ν_{33} (τ_{OH})	242	96	2.52
ν_{32} (ν_{11})	166	166	1.00
ν_{29} (ν_{16a})	419	431	0.97
ν_{31} (ν_{9b})	175	229	0.76
ν_{30} (ν_{5})	107	294	0.36
ν_{28} (ν_{16b})	180	566	0.32
ν_{24} (ν_{17a})	158	891	0.18
ν_{25} (ν_{17b})	133	833	0.16
ν_{27} (ν_{10b})	37	745	0.05
ν_{26} (ν_{10a})	20	775	0.03
4-MeOPhOH			
ν_{43} (τ_{OH})	644	190	3.39
ν_{41} (ν_{16a})	444	385	1.15
ν_{45} ($\tau_{O\text{-}CH3}$)	59	52	1.12
ν_{42} (ν_{10b})	208	263	0.79
ν_{44} (ν_{9b})	90	142	0.64
ν_{39} (ν_{16b})	256	484	0.53
ν_{38} (ν_{10a})	298	750	0.40
ν_{40}	130	414	0.32
ν_{35} (ν_{5})	198	883	0.23
ν_{37} (ν_{17b})	137	792	0.17
ν_{36} (ν_{17a})	49	816	0.06
ν_{34}	14	1189	0.01
ν_{33}	6	1507	0.004
ν_{32}	5	3129	0.001

References

1. W. Domcke and D. R. Yarkony, in *Annual Review of Physical Chemistry*, edited by M. A. Johnson and T. J. Martinez (2012), Vol. 63, pp. 325-352.
2. Z. Lan, A. Dupays, V. Vallet, S. Mahapatra and W. Domcke, J. Photochem. Photobiol. A, 2007, **190**, 177.
3. M. N. R. Ashfold, B. Cronin, A. L. Devine, R. N. Dixon and M. G. D. Nix, Science, 2006, **312**, 1637.
4. M. N. R. Ashfold, A. L. Devine, R. N. Dixon, G. A. King, M. G. D. Nix and T. A. A. Oliver, Proc. Natl. Acad. Sci., 2008, **105**, 12701.
5. M. N. R. Ashfold, G. A. King, D. Murdock, M. G. D. Nix, T. A. A. Oliver and A. G. Sage, Phys. Chem. Chem. Phys., 2010, **12**, 1218.
6. A. Iqbal, L.-J. Pegg and V. G. Stavros, J. Phys. Chem. A, 2008, **112**, 9531.
7. M. Barbatti, B. Sellner, A. J. A. Aquino and H. Lischka, Handbook of Computational Chemistry (Springer, Netherlands), 2008, 209.
8. R. A. Livingstone, J. O. F. Thompson, M. Iljina, R. J. Donaldson, B. J. Sussman, M. J. Paterson and D. Townsend, J. Chem. Phys., 2012, **137**, 184304.
9. J. Wei, A. Kuczmann, J. Riedel, F. Renth and F. Temps, Phys. Chem. Chem. Phys., 2003, **5**, 315.
10. S. Grimme, Chem. Phys., 1992, **163**, 313.
11. A. L. Sobolewski and W. Domcke, Chem. Phys., 2000, **259**, 281
12. A. L. Sobolewski, W. Domcke, C. Dedonder-Lardeux and C. Jouvet, Phys. Chem. Chem. Phys., 2002, **4**, 1093.
13. R. N. Dixon, T. A. A. Oliver and M. N. R. Ashfold, J. Chem. Phys., 2011, **134**, 194303.
14. O. P. J. Vieuxmaire, Z. Lan, A. L. Sobolewski and W. Domcke, J. Chem. Phys., 2008, **129**, 224307.
15. S. G. Ramesh and W. Domcke, Faraday Discuss., 2013, **167**, 73.
16. X. F. Xu, K. R. Yang and D. G. Truhlar, J. Chem. Theory Comput., 2013, **9**, 3612.
17. G. A. Pino, A. N. Oldani, E. Marceca, M. Fujii, S. I. Ishiuchi, M. Miyazaki, M. Broquier, C. Dedonder and C. Jouvet, J. Chem. Phys., 2010, **133**, 124313.
18. G. M. Roberts, A. S. Chatterley, J. D. Young and V. G. Stavros, J. Phys. Chem. Letts., 2012, **3**, 348.
19. T. N. V. Karsili, A. M. Wenge, S. J. Harris, D. Murdock, J. N. Harvey, R. N. Dixon and M. N. R. Ashfold, Chem. Sci., 2013, **4**, 2434.
20. Z. G. Lan, W. Domcke, V. Vallet, A. L. Sobolewski and S. Mahapatra, J. Chem. Phys., 2005, **122**, 224315.
21. G. Berden, L. Meerts, M. Schmitt and K. Kleinermanns, J. Chem. Phys., 1996, **104**, 972.
22. H. D. Bist, J. C. D. Brand and D. R. Williams, J. Mol. Spectrosc., 1967, **24**, 402.
23. S. Albert, P. Lerch, R. Prentner and M. Quack, Angew. Chem. Int. Ed., 2013, **52**, 346.

24. M. G. D. Nix, A. L. Devine, B. Cronin, R. N. Dixon and M. N. R. Ashfold, J. Chem. Phys., 2006, **125**, 133318.
25. G. A. King, T. A. A. Oliver, M. G. D. Nix and M. N. R. Ashfold, J. Phys. Chem. A, 2009, **113**, 7984.
26. A. L. Devine, M. G. D. Nix, B. Cronin and M. N. R. Ashfold, Phys. Chem. Chem. Phys., 2007, **9**, 3749.
27. G. A. King, A. L. Devine, M. G. D. Nix, D. E. Kelly and M. N. R. Ashfold, Phys. Chem. Chem. Phys., 2008, **10**, 6417.
28. T. A. A. Oliver, G. A. King and M. N. R. Ashfold, Phys. Chem. Chem. Phys., 2011, **13**, 14646.
29. B. Cronin, M. G. D. Nix, R. H. Qadiri and M. N. R. Ashfold, Phys. Chem. Chem. Phys., 2004, **6**, 5031.
30. L. Schnieder, W. Meier, K. H. Welge, M. N. R. Ashfold and C. M. Western, J. Chem. Phys., 1990, **92**, 7027.
31. H. J. Werner, P. J. Knowles, G. Knizia, F. R. Manby, M. Schütz, P. Celani, T. Korona, R. Lindh, A. Mitrushenkov, G. Rauhut, K. R. Shamasundar, T. B. Adler, R. D. Amos, A. Bernhardsson, A. Berning, D. L. Cooper, M. J. O. Deegan, A. J. Dobbyn, F. Eckert, E. Goll, C. Hampel, A. Hesselmann, G. Hetzer, T. Hrenar, G. Jansen, C. Köppl, Y. Liu, A. W. Lloyd, R. A. Mata, A. J. May, S. J. McNicholas, W. Meyer, M. E. Mura, A. Nicklass, D. P. O'Neill, P. Palmieri, K. Pflüger, R. Pitzer, M. Reiher, T. Shiozaki, H. Stoll, A. J. Stone, R. Tarroni, T. Thorsteinsson, M. Wang and A. Wolf, MOLPRO, version 2010.1, a package of ab initio programs, 2010.
32. T. H. Dunning, Jr., J. Chem. Phys., 1989, **90**, 1007.
33. M. J. Frisch, G. W. Trucks, H. B. Schlegel, G. E. Scuseria, M. A. Robb, J. R. Cheeseman, J. A. Montgomery, Jr. , T. Vreven, K. N. Kudin, J. C. Burant, J. M. Millam, S. S. Iyengar, J. Tomasi, V. Barone, B. Mennucci, M. Cossi, G. Scalmani, N. Rega, G. A. Petersson, H. Nakatsuji, M. Hada, M. Ehara, K. Toyota, R. Fukuda, J. Hasegawa, M. Ishida, T. Nakajima, Y. Honda, O. Kitao, H. Nakai, M. Klene, X. Li, J. E. Knox, H. P. Hratchian, J. B. Cross, C. Adamo, J. Jaramillo, R. Gomperts, R. E. Stratmann, O. Yazyev, A. J. Austin, R. Cammi, C. Pomelli, J. W. Ochterski, P. Y. Ayala, K. Morokuma, G. A. Voth, P. Salvador, J. J. Dannenberg, V. G. Zakrzewski, S. Dapprich, A. D. Daniels, M. C. Strain, O. Farkas, D. K. Malick, A. D. Rabuck, K. Raghavachari, J. B. Foresman, J. V. Ortiz, Q. Cui, A. G. Baboul, S. Clifford, J. Cioslowski, B. B. Stefanov, G. Liu, A. Liashenko, P. Piskorz, I. Komaromi, R. L. Martin, D. J. Fox, T. Keith, M. A. Al-Laham, C. Y. Peng, A. Nanayakkara, M. Challacombe, P. M. W. Gill, B. Johnson, W. Chen, M. W. Wong, C. Gonzalez and J. A. Pople, Gaussian Inc., 2004.
34. T. S. Venkatesan, S. G. Ramesh, Z. Lan and W. Domcke, J. Chem. Phys., 2012, **136**, 174312.
35. H. Köppel, W. Domcke and L. S. Cederbaum, Adv. Chem. Phys., 1984, **57**, 59.
36. A. L. Devine, B. Cronin, M. G. D. Nix and M. N. R. Ashfold, J. Chem. Phys., 2006, **125**, 184302.

37. D. J. Hadden, G. M. Roberts, T. N. V. Karsili, M. N. R. Ashfold and V. G. Stavros, Phys. Chem. Chem. Phys., 2012, **14**, 13415.
38. G. Versanyi, Vibrational Spectra of Benzene Derivatives, Wiley, New York., 1974.
39. G. Herzberg, Electronic Spectra of Polyatomic Molecules, D. Van Nostrand Company, Inc., Princeton , 1966.
40. G. N. Patwari, S. Doraiswamy and S. Wategaonkar, J. Phys. Chem. A, 2000, **104**, 8466.

Figure 1

Unrelaxed PECs along $R_{O–H}$ for the ground and first two excited singlet states of (a) 4-FPhOH, (b) 3-FPhOH and (c) 4-MeOPhOH calculated at the CASPT2 level of theory.

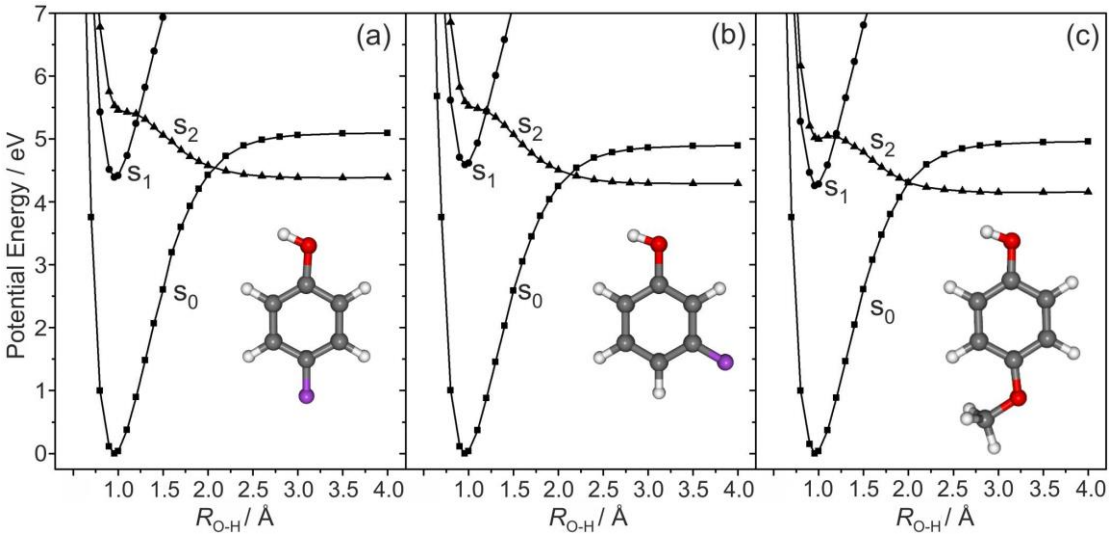

Figure 2

1+1 REMPI spectra of jet-cooled samples of (a) 3-FPhOH and (b) 4-MeOPhOH. Peak assignments for the latter are from the earlier work of Patwari *et al*.[36]

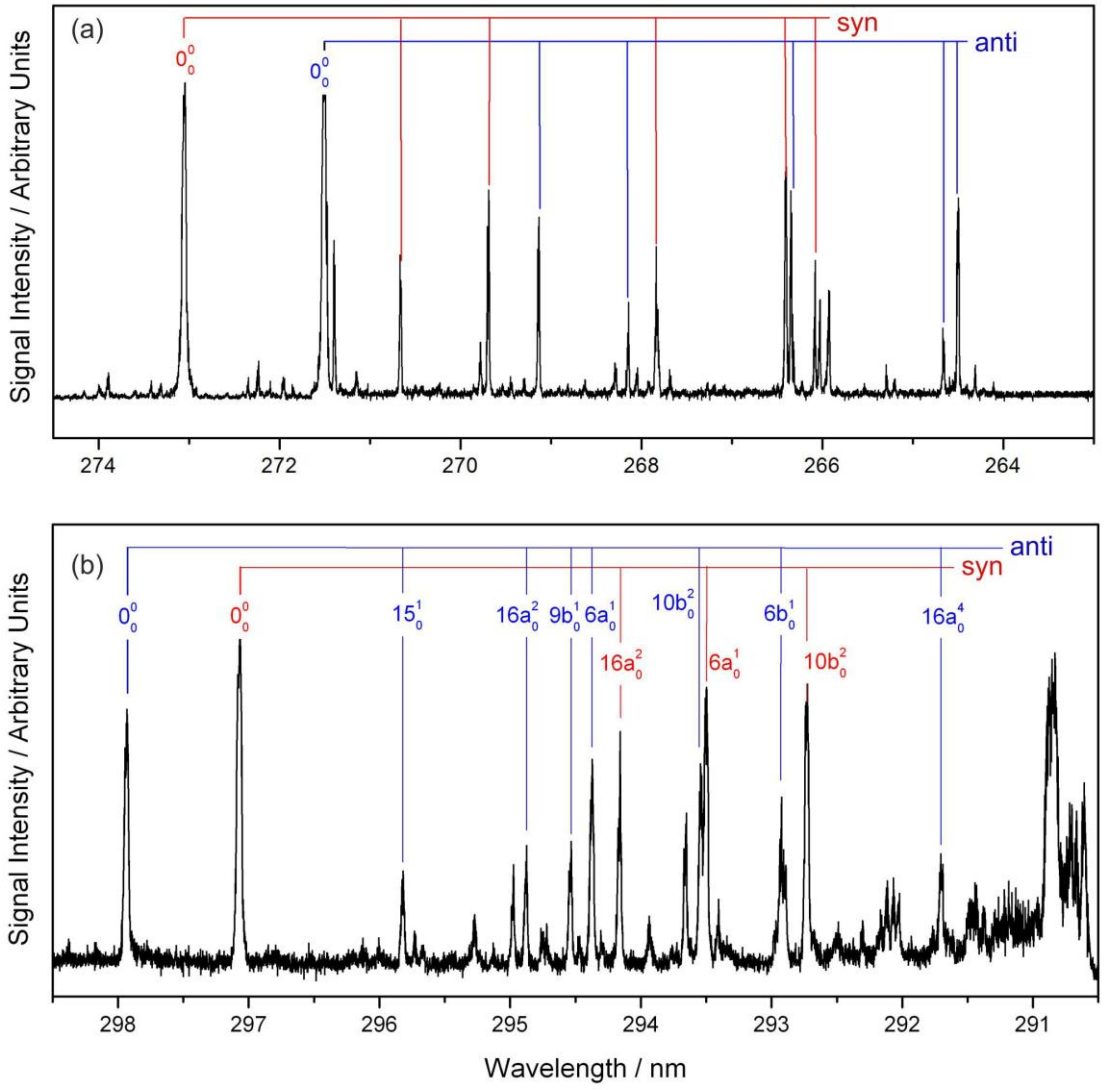

Figure 3

TKER spectra derived from H atom TOF spectra measured when exciting (a) PhOH, (b) 4-FPhOH, (c) *syn*-3-FPhOH, (d) *anti*-3-FPhOH, (e) *syn*-4-MeOPhOH and (f) *anti*-4-MeOPhOH on the respective S_1–S_0 origin transitions. The feature identified as the $TKER_{max}$ peak is indicated in each case.

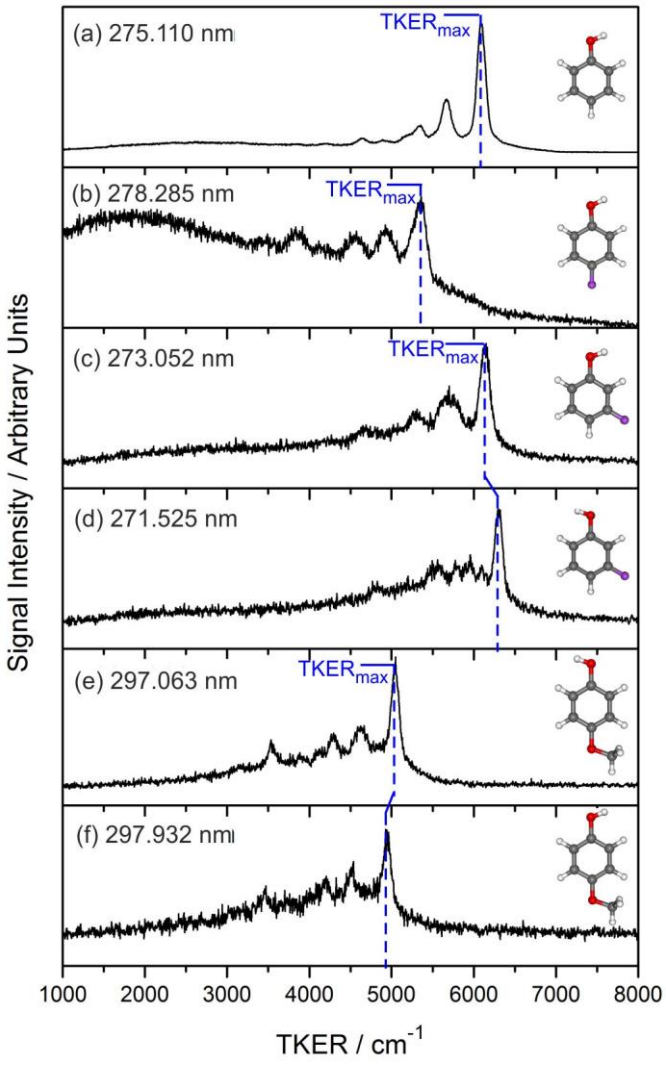

Figure 4

TKER spectra derived from H atom TOF spectra measured when exciting (a) PhOH, (b) 4-FPhOH, (c) 3-FPhOH and (d) 4-MeOPhOH at energies above the respective S_1/S_2 CIs. The feature identified as the $TKER_{max}$ peak is indicated in each case.

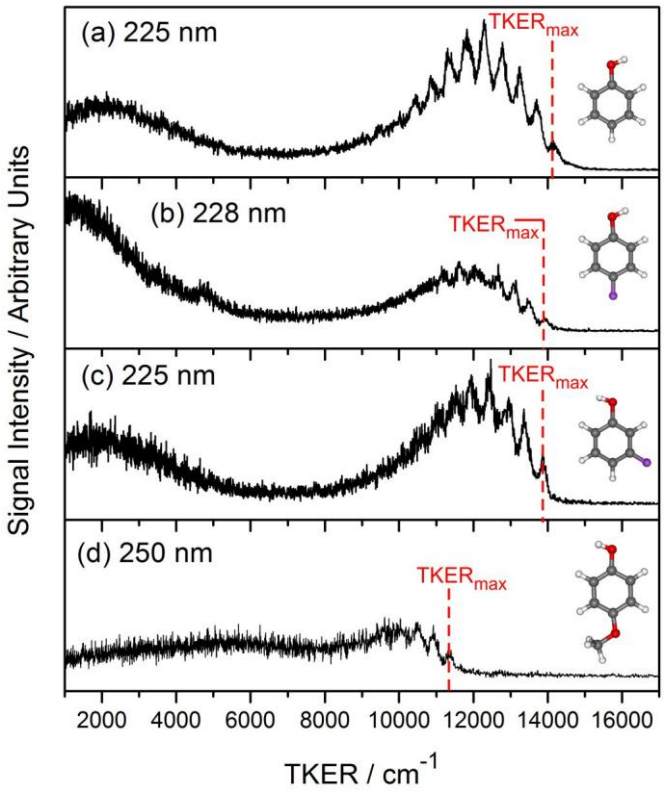

Figure 5

Plots of $TKER_{max}$ *vs* E_{phot} for (a) PhOH and (b) 3-FPhOH. Lines of best-fit with unit gradient are superposed on each plot; the dashed lines in (a) are extrapolations of the best-fit line through the data recorded in the other wavelength region, which serve to illustrate that the $TKER_{max}$ peaks cannot all associate with a common H + PhO(X),v product channel. The long wavelength data points in panel (b) are distinguished according to whether the resonance excited is attributed to the *syn*- (o) or *anti*-rotamer (•).

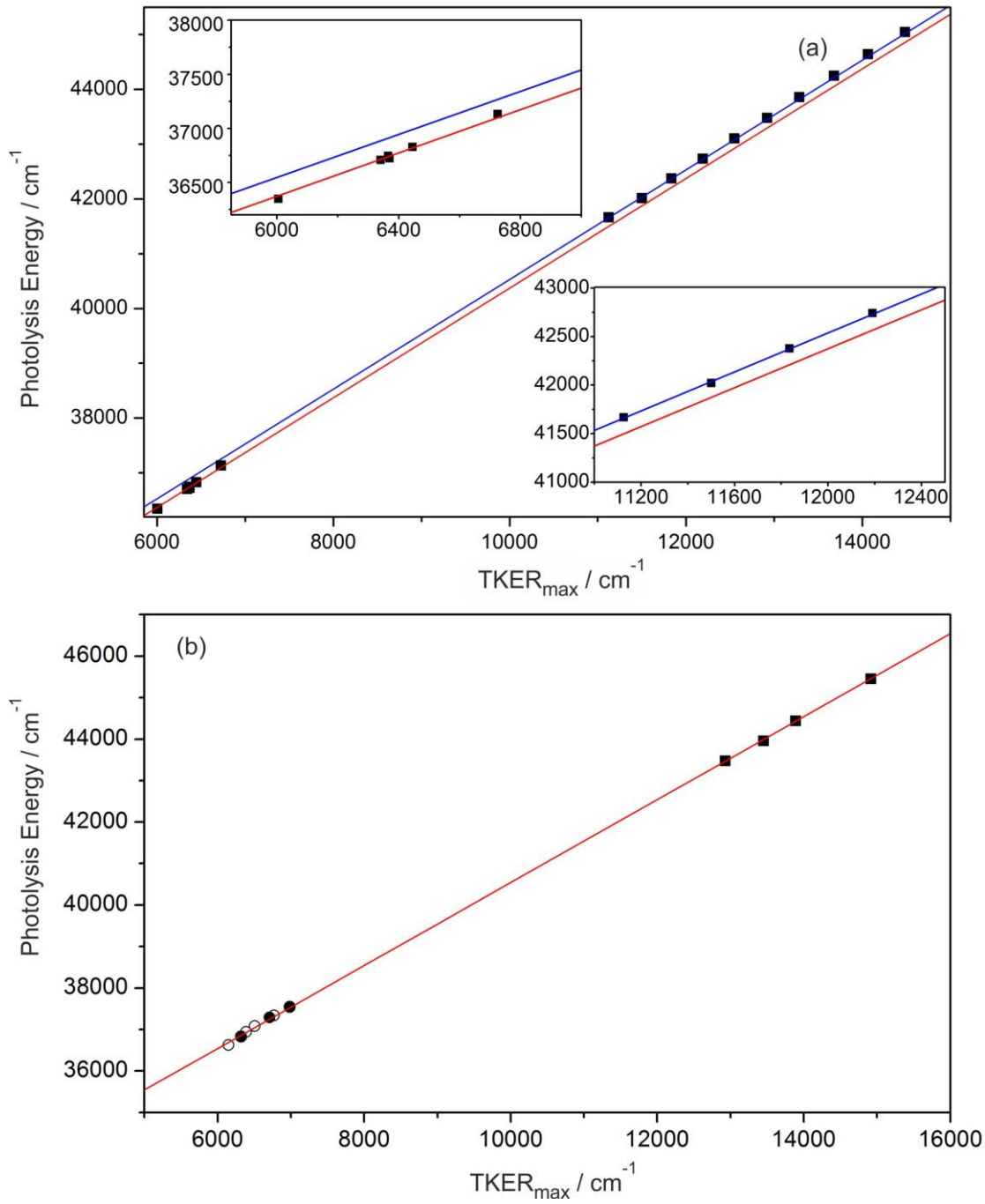
(a)
Photolysis Energy / cm-1
TKERmax / cm-1
38000
37500
37000
36500
6000
6400
6800
43000
42500
42000
41500
41000
11200
11600
12000
12400
44000
42000
40000
38000
6000
8000
10000
12000
14000
(b)
Photolysis Energy / cm-1
TKERmax / cm-1
46000
44000
42000
40000
38000
36000
6000
8000
10000
12000
14000
16000

Figure 6

1-D PECs through the S_1 and S_2 PESs of (a-c) 4-FPhOH and (d-f) 3-FPhOH calculated at the EOM-CCSD/cc-pVTZ level as functions of selected Q_x (of a_2 (a") symmetry) in order of decreasing coupling strength (λ_x/ω_x).

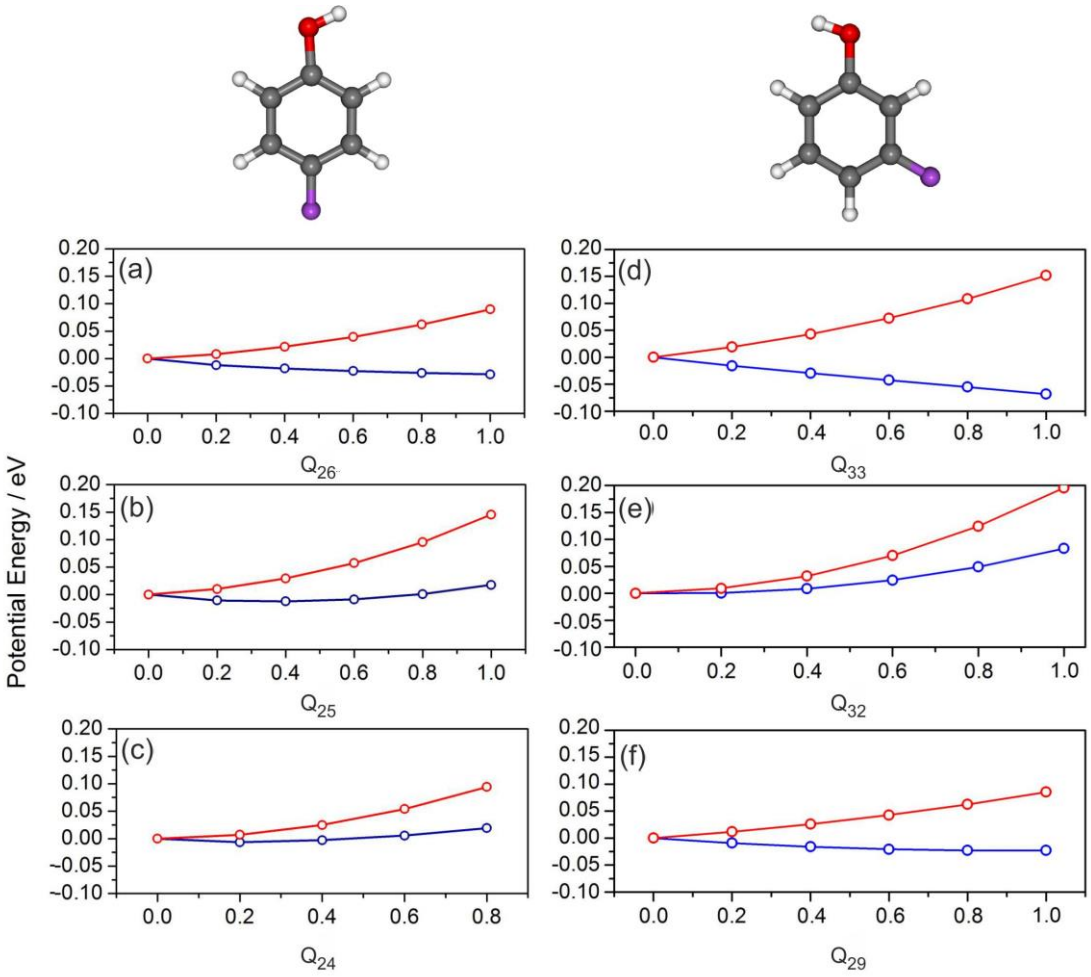

Figure 7

E_{int} spectra of the 3-FPhO(X) radicals formed by photolysis of jet-cooled 3-FPhOH molecules on selected resonances within the S_1–S_0 band shown in fig. 2(a).

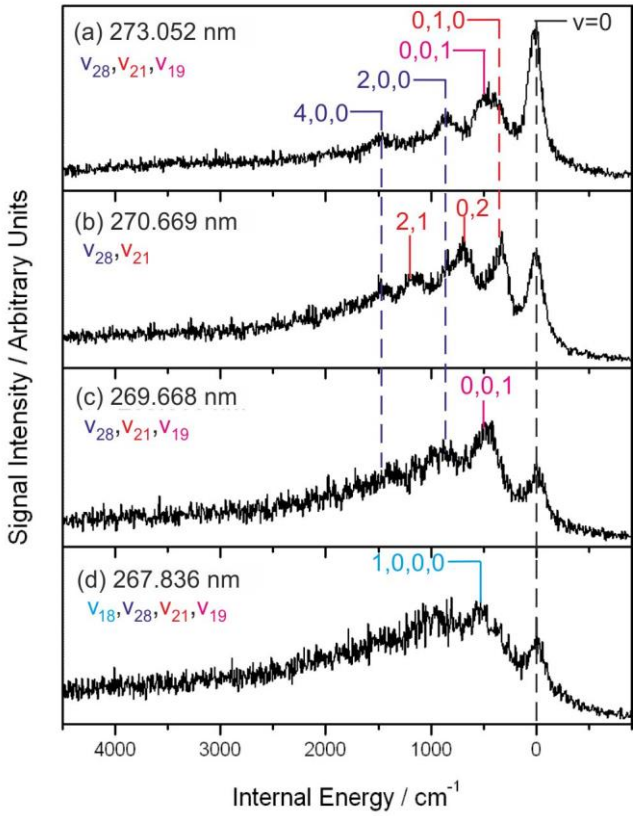

Figure 8

E_{int} spectra of the 3-FPhO(X) radicals formed by photolysis of jet-cooled 3-FPhOH molecules at various λ_{phot} corresponding to energies above the S_1/S_2 CI.